

# Deep multi-stations weather forecasting: explainable recurrent convolutional neural networks

Ismail Alaoui Abdellaoui, Siamak Mehrkanoon\*

Department of Data Science and Knowledge Engineering, Maastricht University, The Netherlands

## Abstract

Deep learning applied to weather forecasting has started gaining popularity because of the progress achieved by data-driven models. The present paper compares four different deep learning architectures to perform weather prediction on daily data gathered from 18 cities across Europe and spanned over a period of 15 years. The four proposed models investigate the different type of input representations (i.e. tensorial unistream vs. multi-stream matrices) as well as the combination of convolutional neural networks and LSTM (i.e. cascaded vs. ConvLSTM). In particular, we show that a model that uses a multi-stream input representation and that processes each lag individually combined with a cascaded convolution and LSTM is capable of better forecasting than the other compared models. In addition, we show that visualization techniques such as occlusion analysis and score maximization can give an additional insight on the most important features and cities for predicting a particular target feature and city.

**Keywords:** Weather data, deep learning, convolutional neural network, LSTM, explainability

## 1. Introduction

Weather forecasting is of major importance as it affects the daily activities of fundamental fields such as agriculture, transportation and international commerce among others. The ability to forecast the precipitation rates, the risk of flood or the likelihood of a hurricane can potentially lead to saving of lives and to the well-being of humans. Moreover, the change of the climate on earth has led to increasing research and world-wide efforts to halt the environmental and ecological consequences [26].

Traditional approaches of weather forecasting rely on priors like the thermodynamic properties of the atmosphere [12, 25, 5], statistical distribution of the data [9], or ensemble learning that incorporates multiple models with different initial conditions [10]. This family of models belongs to the “Numerical Weather Prediction” (NWP) methodologies [15] and usually rely on the processing power of supercomputers, thus being resource heavy [2]. In addition of the high computational cost, it has been shown that *a priori* information about the data that constitutes the initial state is the source of errors in weather prediction [29].

While traditional NWP methods aim at extracting useful dynamics from a model or to transfer information between models, the purpose of recent data-driven approaches is to simulate an entire system to predict its future state [27]. Machine learning data driven based models have already been successfully applied in various domains such as healthcare, dynamical systems, biomedical signal analysis, neuroscience among others [20, 22, 21, 18, 23, 1, 4, 32, 17]. The recent advances of

machine learning models has increased the capability to automatically learn the underlying nonlinear complex patterns of weather dynamics [19, 30, 31]. In particular, the combination of convolutional neural networks (CNNs) and long short-term memory (LSTM) networks proved to be a successful deep learning approach for climate modeling and weather forecasting [6, 8].

This paper presents two contributions. The first one is an investigation of the Conv-LSTM network for weather forecasting. More specifically, within the context of weather forecasting, we are examining whether the convolution operations should happen within the LSTM cells or outside, in a consecutive fashion. Another analysis aims at determining the impact of a tensorial versus a matrix-based input representation fed to the networks. The second contribution aims at using modern visualization techniques to determine the features and cities that contribute the most to the output predictions of a particular city or group of cities. It is of utter importance to gain interpretability from the data driven models given that weather predictions potentially is the basis of many human real-life decisions.

This paper is organized as follows. A brief review of the existing machine learning methodologies for weather forecasting is given in Section 2. A formal definition of the Conv-LSTM layer and the visualization techniques used are presented in Section 3. Our proposed models are introduced in Section 4. Furthermore, the dataset used is introduced in Section 5. The experimental results are reported in section 6. Finally, a discussion followed by the conclusion are drawn in sections 7 and 8, respectively.

\*Corresponding author

## 2. Related Work

Multiple approaches have been recently proposed to tackle weather forecasting using deep machine learning models. The author in [19] introduced the convolutional neural networks to learn the underlying spatio-temporal patterns of weather data. This work used hourly past data from cities in the Netherlands, Belgium and Denmark to predict the temperature and wind speed of multiple cities. It has been shown that the convolutional operations benefit from a tensorial representation in order to improve the prediction capability.

In another work, a feed forward neural network has been used to investigate the volume of data needed as well as its recency to yield accurate weather predictions. In terms of data volume, it has been shown that more data consistently leads to better predictions. The impact of the data recency remains unknown as there was no significant impact on the predictions when tuning the recency of the data [3].

In [34], the authors used deep learning to predict weather phenomena related to the heating of the air (i.e. heavy rains and thunderstorms among others), more commonly known as severe convective weather (SCW). A deep CNN has been utilized and proved to yield superior results compared to traditional machine learning models such as support vector machines or random forests. Another model which used stacked ConvLSTM layers, *DeepRain*, was compared to linear regression models and reduced the RMSE by a large margin. This model used past radar data with a 6-min time resolution over a period of two years [13].

Similarly to the previous work, the authors in [28] used a multi-input network with past radar data to perform precipitation forecasting. However, a different approach was used since the regression problem was transformed into a multi-class classification of possible precipitation ranges. The model also made use of axial self-attention [11] as spatial aggregator. This model was able to outperform the system used in the National Oceanic and Atmospheric Administration (NOAA). In [7], the different challenges of using deep learning for weather forecasting are addressed. In particular, it has been stated that while neural networks can be useful for short-term predictions, the need for domain knowledge is essential when tackling forecasting of longer term ranges.

## 3. Preliminaries

### 3.1. Conv-LSTM

In this section we give an overview of the ConvLSTM layer. It is based on the LSTM cell and was introduced in [33] to address the issue of capturing the spatial structure of the data. In this model, the input gate  $i_t$ , the forget gate  $f_t$ , the output gate  $o_t$ , the hidden state  $h_{t-1}$ , the candidate cell state  $\hat{C}_t$ , the current cell state  $C_t$  and the input  $x_t$  are all 3D tensors. The first dimension of each tensor is the sequence length while the two last dimensions represent the rows and columns. This model has first been used on weather data for precipitation nowcasting, outperforming other models based on the LSTM only.

### 3.2. Activation maximization

Activation maximization is a visualization technique that looks for patterns that maximize a particular activation function inside a neural network [16]. Following the taxonomy of interpretability methods presented in [24], activation maximization is a post hoc method since it aims at understanding the model after the training. This methodology focuses on finding a new input that maximizes the activation of a neuron:

$$I^* = \underset{I}{\operatorname{argmax}} h_{l,z}(I), \quad (1)$$

where  $I$  is the input data of the network,  $h$  is the activation function used in the neuron  $z$  of the layer index  $l$ . For our case, we want to find the input data that contributes the most to minimizing the error between the model prediction and ground truth data. Since in our study weather element forecasting is reduced to a regression problem, here we define  $h$ , a custom objective function, as the inverse of the mean squared error (MSE):

$$h = \frac{1}{\frac{1}{n} \sum_{i=1}^n (y_i - \hat{y}_i)^2}, \quad (2)$$

where  $y_i$  and  $\hat{y}_i$  are the true measured data and the model prediction of a particular weather feature for the  $i^{\text{th}}$  target city. Here,  $n$  denotes the number of target cities. The pseudocode of maximizing the  $h$  score and getting the score map  $I^*$  is provided in Algorithm 1.

---

#### Algorithm 1: Score Maximization

---

**Input:** The number of iterations  $s$

Pretrained model  $m_p$

Sample input  $I$

Input ranges  $I_{\min}$  and  $I_{\max}$

Learning rate  $\eta$

**Output:** New input  $I^*$

**for** the number of iterations  $s$  **do**

    Perform a forward pass of  $m_p$  on  $I$  to get a prediction  $\hat{y}$ .

    Use eq. (2) to obtain the score  $h$ .

    Apply  $L_2$  normalization on the obtained score.

    Compute the gradient  $dI$  of the normalized score with respect to input  $I$ .

    Update the input using:  $I \leftarrow I + \eta dI$ .

**end**

Obtain  $I^*$  by clipping  $I$  based on  $I_{\min}$  and  $I_{\max}$ .

---

### 3.3. Occlusion Analysis

The occlusion analysis is a simplistic, yet effective way to determine which features contribute the most to a minimal error between the actual and prediction data. In this paper, we are concerned with two types of occlusion analysis: a spatial and a temporal occlusion. While the spatial occlusion analysis focuses on the important cities and weather features, the temporal analysis aims at determining the most important lags. The spatial occlusion analysis can be used to either focus on the

cities only, or on the weather features only, or on a group of cities and features. However, all of these approaches rely on the same principle, which is to compute the percentage change between a reference MSE, obtained from the prediction of an unmasked data sample and its corresponding ground truth target data, and a new MSE, computed from the prediction of a masked data sample and the same ground truth label. We perform this percentage change each time the mask is slid to a new location of the input. Focusing on either the cities or the weather features on one hand, or a group of cities and features on the other hand, will determine the shape of the mask (i.e. a vector or a matrix, respectively). We present in Algorithm 2 the specific pseudocode of the occlusion analysis, when using a square matrix of size  $p$  as a mask over the input dataset  $\mathcal{X}$ , and for a particular target city.

---

**Algorithm 2:** Occlusion analysis

---

**Input:** Input dataset  $\mathcal{X} = \{x_i\}_{i=1}^k$   
Target dataset  $\mathcal{O} = \{o_i\}_{i=1}^k$   
Pretrained model  $m_p$   
Target city index  $c$   
Mask size  $p$   
Number of horizontal slidings  $s_h$   
Number of vertical slidings  $s_v$

**Output:** Occlusion map  $M_o$

```

for the number of data samples do
  Perform a prediction of the sample  $x_i$  using  $m_p$ .
  Compute  $MSE_i$  between the real target data  $o_i$  and
  the model prediction for the  $c^{th}$  city.
  for the number of horizontal slidings  $s_h$  do
    for the number of vertical slidings  $s_v$  do
      Mask the sample  $x_i$  by the patch to get the
      masked sample  $\tilde{x}_i$ .
      Make a new prediction using masked sample
       $\tilde{x}_i$ .
      Compute the  $\widetilde{MSE}_i$  between  $o_i$  and the
      recent model prediction for the  $c^{th}$  city.
      Calculate the percentage change  $\Delta$  between
       $MSE_i$  and  $\widetilde{MSE}_i$ .
      Store  $\Delta$  in a tensor  $\mathcal{M}$  for this particular
      patch location.
      Displace the mask vertically by the distance
       $p$  over the sample  $x_i$ .
    end
    Displace the mask horizontally by the distance  $p$ 
    over the sample  $x_i$ .
  end
end

```

For each mask location, compute an average of the stored  $\Delta$  over all data samples from  $\mathcal{M}$  to get the occlusion map  $M_o$ .

---

## 4. Proposed Models

The four proposed models aim at studying how the convolutional and recurrent layers perform at weather forecasting, as well as investigating the impact of the input representation. To this end, the four models use three types of layers: convolutional, LSTM, and ConvLSTM layers. Additionally, two types of input representations are used: a unistream tensorial representation and a multi-stream representation that uses matrices.

### 4.1. Conv + LSTM model (Conv+LSTM)

This model uses a tensor input representation combined with convolutional and LSTM layers. The input of the model is a tensor  $\mathcal{T} \in \mathbb{R}^{L \times F \times C}$  where  $L$  is the number of lags used,  $F$  is the number of weather features, and  $C$  the number of cities. The architecture consists of three 2D convolutional layers, followed by two LSTM layers. The last LSTM layer returns the last hidden state. A dense layer is then used before the final output layer.

### 4.2. ConvLSTM model (ConvLSTM)

This model uses the same tensor input representation  $\mathcal{T}$  described above. However the layer used is a ConvLSTM layer presented in section 3.1. This layer is followed by two dense layers before the output layer.

### 4.3. Multi-Stream Conv+LSTM model (MS-Conv+LSTM)

This model uses a multi-stream approach where each stream processes an input matrix  $M_t \in \mathbb{R}^{F \times C}$ . Therefore the number of streams is equivalent to the number of lags used in the first two models, meaning that this model processes each lag individually. Each stream is made of four 2D convolutional layers. The output of each stream is then concatenated to form the input sequence for the LSTM layer. Unlike the Conv+LSTM model, only one LSTM layer is used as it empirically proved to yield better results. Finally one dense layer follows the recurrent layer before the final prediction.

### 4.4. Multi-Stream ConvLSTM model (MS-ConvLSTM)

Similarly to the MS-Conv+LSTM model, this architecture uses a multi-stream architecture. However, each input stream is a tensor  $\mathcal{U} \in \mathbb{R}^{V \times F \times C}$  where  $V$  is the number of lags used in each tensor. Since all the models use the same number of lags, then  $V$  evenly divides the total number of lags  $L$  in each sample. Two ConvLSTM layers are used in each stream to capture the spatial and temporal features. The output of each stream is then concatenated and processed by a dense layer before the final output layer.

Fig. 1 shows the schema of the proposed four models. The output of these models is a vector  $o$  of length  $n$ , i.e. the number of target cities. Each value in this vector represents the same target feature for all the target cities. The hyperparameters of these models were selected so that they all have a comparable number of learnable parameters as shown in Table 1.

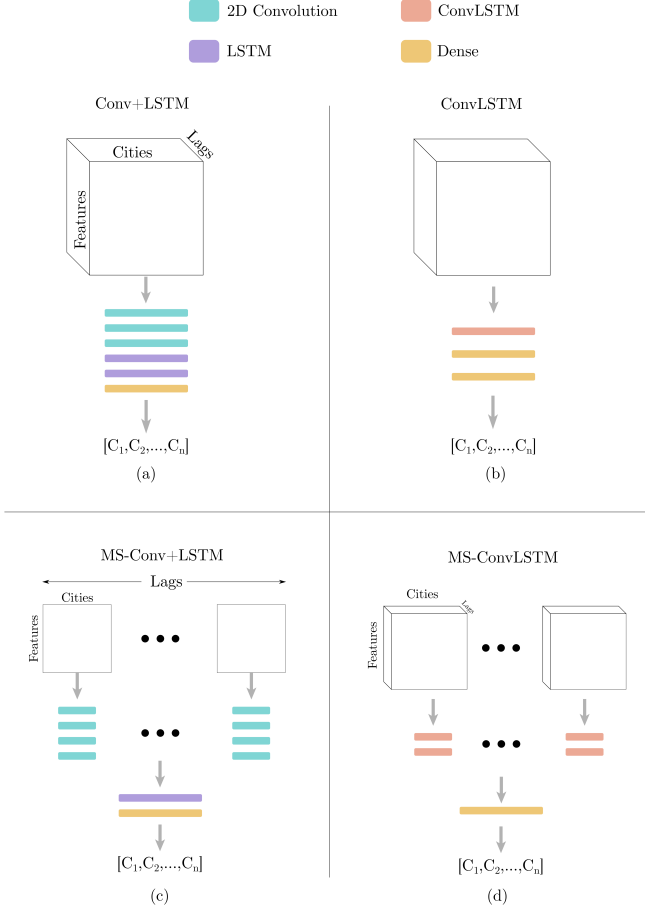


**Figure 1:** Schemas of the 4 different models. The top row shows the schemas of (a) the Conv+LSTM and (b) ConvLSTM models while the bottom row displays the (c) MS-Conv+LSTM and (d) MS-ConvLSTM models.

Table 1: Parameters of the four models.

Model	Parameters
Conv+LSTM	337,271
ConvLSTM	330,621
MS-Conv+LSTM	373,716
MS-ConvLSTM	401,556

## 5. Data Description

The dataset used has been collected from Weather Underground and includes 18 cities across Europe and 18 weather features, for a period of 15 years from May 2005 to April 2020. Its time resolution is daily and weather features include for instance the temperature, wind speed, condition and sea level pressure among others. Table 2 presents the list of all features used. At each time step  $t$ , a data sample is represented by a matrix  $M_t \in \mathbb{R}^{F \times C}$ , where  $F$  is the number of features and  $C$  is the number of cities. Therefore the whole dataset is a tensor  $\mathcal{D} \in \mathbb{R}^{L \times F \times C}$ , where  $L$  is the total number of days used. Fig. 2

shows a map of different cities that are contained in the dataset.

Table 2: Features used in the dataset.

Feature name	Remarks
Highest temperature (°F)	-
Lowest temperature (°F)	-
Average temperature (°F)	-
Dew point (°F)	-
Highest dew point (°F)	-
Lowest dew point (°F)	-
Average dew point (°F)	-
Maximum wind speed (mph)	-
Visibility (mi)	Discrete value expressed in miles to measure the distance at which an object can be clearly distinguished
Sea level pressure (Hg)	Measured in inch of mercury
Observed temperature (°F)	Temperature in Fahrenheit observed at 10 am
Observed dew point (°F)	Dew point in Fahrenheit observed at 10 am
Humidity (%)	-
Wind direction	Discrete values indicating 16 possible directions of the wind
Wind speed (mph)	-
Wind gust (mph)	-
Pressure (in)	-
Condition	21 possible discrete values that describe the overall weather state (cloudy, rainy, fog ...)



**Figure 2:** Map showing the 18 cities used in the dataset.

## 6. Experimental Results

### 6.1. Data Preprocessing

The weather data is first scaled by means of equation 3. In this way, for each feature and city, we take the values corresponding to every date and scale them down between 0 and 1.

$$x_{scaled} = \frac{x - \min(c_{ij})}{\max(c_{ij}) - \min(c_{ij})}, i \in [1, F], j \in [1, C], \quad (3)$$

where  $c_{ij} \in \mathbb{R}^L$  refers to a column vector and  $i$  and  $j$  are the  $i^{\text{th}}$  feature of the  $j^{\text{th}}$  city.

### 6.2. Experimental setup

For all the experiments, the following six cities have been used as target cities: Paris, Luxembourg, London, Brussels, Frankfurt and Rotterdam. We also selected two target features: the wind speed, in miles per hour, and the average temperature of the day, in degree Fahrenheit. It should be noted that for each training instance, the output vector corresponds to only one type of feature, for all the target cities. Moreover, we performed experiments for 2, 4 and 6 days ahead, using 10 lags. All the experiments used 90% of the data for training and validation, while the remaining 10% was used for testing. Adam method [14] is used to optimize the mean square error (MSE) with a learning rate of  $1e^{-4}$  and a batch size of 16 for all of the proposed models.

### 6.3. Results

The obtained mean squared error (MSE) of the proposed four models for wind speed as well as average temperature prediction for six target cities over 2, 4, and 6 days ahead are tabulated in Table 3 and Table 4 respectively. For every city and days ahead, the MSE of the best model is underlined. It should be noted that the reported MSEs are calculated after descaling the models prediction.

Table 3: The MSE comparison of the four models, for 2, 4, and 6 days ahead **wind speed** prediction.

Days ahead	City	Conv+LSTM	ConvLSTM	MS-Conv+LSTM	MS-ConvLSTM
2	Luxembourg	26.65	28.85	<u>24.48</u>	26.94
	Rotterdam	44.38	48.04	<u>40.76</u>	44.85
	Frankfurt	37.97	41.11	<u>34.87</u>	38.38
	Brussels	33.98	36.78	<u>31.21</u>	34.34
	London	28.40	30.75	<u>26.08</u>	28.71
	Paris	23.32	25.25	<u>21.42</u>	23.58
4	Luxembourg	29.98	32.27	31.54	<u>29.85</u>
	Rotterdam	49.92	53.73	52.52	<u>49.69</u>
	Frankfurt	42.71	45.97	44.93	<u>42.52</u>
	Brussels	38.22	41.14	40.21	<u>38.05</u>
	London	31.95	34.39	33.61	<u>31.80</u>
	Paris	26.24	28.24	27.60	<u>26.12</u>
6	Luxembourg	31.88	38.22	32.76	<u>30.63</u>
	Rotterdam	53.07	63.64	54.53	<u>51.00</u>
	Frankfurt	45.41	54.45	46.66	<u>43.64</u>
	Brussels	40.63	48.72	41.75	<u>39.05</u>
	London	33.97	40.73	34.90	<u>32.64</u>
	Paris	27.90	33.45	28.66	<u>26.81</u>

From Tables 3 and 4, one can observe that the third and fourth models are the most successful ones. This suggests that in general the multi-stream approach seems better than the tensorial input representation for this particular task. However, if one considers each feature prediction separately, we can distinguish more specific patterns. As it is shown in Table 3, which displays the forecasting results of the wind speed, the multi-stream approach consistently yields a better performance than the tensorial input representation. Moreover, the MS-Conv+LSTM seems to favor short term predictions while the MS-ConvLSTM yields the best results when tackling longer term predictions. Indeed, the stacked recurrent convolutional network outperforms the other models in the 2 days ahead prediction while the network that makes use of the ConvLSTM architecture consistently yields the lowest MSE for the 4 days and 6 days ahead predictions. Similarly, if one considers Table 4 only, the MS-Conv+LSTM model performs better than the other models for

short and medium term predictions (i.e. 2 and 4 days ahead). Interestingly enough, the Conv+LSTM model outperforms the other models in the 6 days ahead prediction. It should also be noted that the MSEs of the wind speed are generally smaller than the ones corresponding to the average temperature. Despite the cyclical nature of temperature, the proposed models seem to better grasp the pattern of the wind speed. Finally, while it seems that Paris' wind speed is the easiest feature and city to predict, it appears that Brussels average temperature is the one yielding the smallest MSE among other tested cities.

Table 4: The MSE comparison of the four models, for 2, 4, and 6 days ahead **average temperature** prediction.

Days ahead	City	Conv+LSTM	ConvLSTM	MS-Conv+LSTM	MS-ConvLSTM
2	Luxembourg	33.20	58.40	<u>26.88</u>	46.35
	Rotterdam	30.07	52.89	<u>24.35</u>	41.98
	Frankfurt	30.54	53.73	<u>24.73</u>	42.65
	Brussels	24.37	42.87	<u>19.73</u>	34.02
	London	25.47	44.80	<u>20.62</u>	35.56
	Paris	30.22	53.15	<u>24.46</u>	42.19
4	Luxembourg	49.00	67.71	<u>45.83</u>	59.41
	Rotterdam	44.37	61.32	<u>41.51</u>	53.81
	Frankfurt	45.08	62.29	<u>42.17</u>	54.66
	Brussels	35.96	49.70	<u>33.64</u>	43.61
	London	37.59	51.94	<u>35.16</u>	45.58
	Paris	44.59	61.62	<u>41.71</u>	54.07
6	Luxembourg	<u>53.38</u>	75.87	64.01	65.96
	Rotterdam	<u>48.35</u>	68.72	57.97	59.74
	Frankfurt	<u>49.11</u>	69.80	58.88	60.68
	Brussels	<u>39.18</u>	55.69	46.98	48.41
	London	<u>40.95</u>	58.20	49.10	50.60
	Paris	<u>48.59</u>	69.05	58.25	60.03

Another interesting analysis is based on pairwise comparisons between the models in order to determine which architecture and input representation to the network performs better for this particular task. For instance, by comparing the first two models across all results one can see that the cascaded configuration is better when using a tensorial input representation. Indeed, for the majority of the results, it is most likely that the Conv+LSTM model will make a better forecasting since the majority of the results of this model yield a lower MSE (95% for the Conv+LSTM versus 5% for the ConvLSTM).

Similarly, comparing the first and third models allow us to infer which input representation yields the best results, since both of the models use convolutional and LSTM layers in a consecutive fashion. One can observe that the input representation does not make a difference. Moreover, comparing the second and fourth models allow us to determine which input representation is better when using the ConvLSTM layers. A multi-stream input representation is clearly more suitable for this task since the fourth model performed better than the second one. Indeed, the multi-stream model made a better forecasting, i.e. 95% of the time for this particular pairwise comparison. Finally, we can also compare the third and fourth models to determine which convolutional recurrent approach is better if a multi-stream representation is used. As suggested from the previous comparisons, a cascaded convolutional recurrent configuration performs better than the ConvLSTM layers (67% for the cascaded configuration versus 33% for the ConvLSTM layers). Fig. 4 displays the pairwise comparison discussed above for the studied dataset. Moreover, Fig. 3 shows the result of real data versus its prediction for 2, 4 and 6 days ahead for the MS-

Conv+LSTM model. The descaled data of the prediction uses the scaling information (i.e. maximum and minimum) from the training samples.

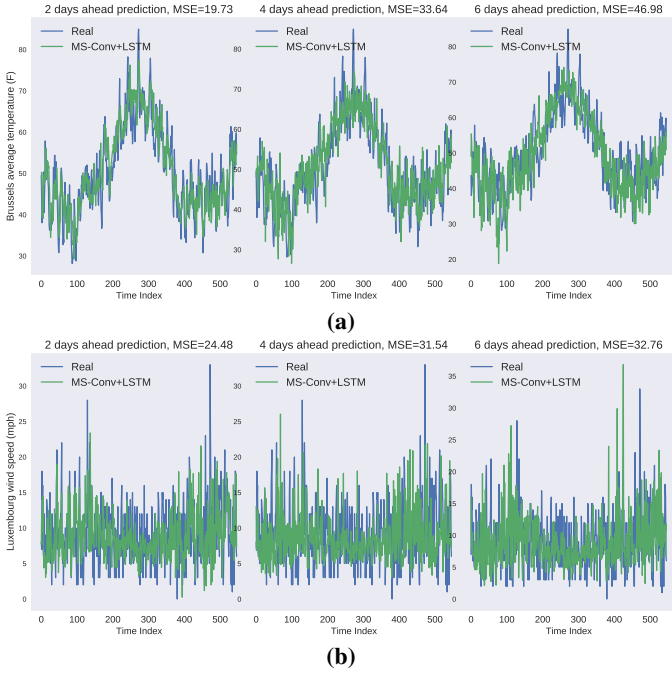


**Figure 3:** Actual vs. prediction of the average temperature (a) and wind speed (b) using the MS-Conv+LSTM model.

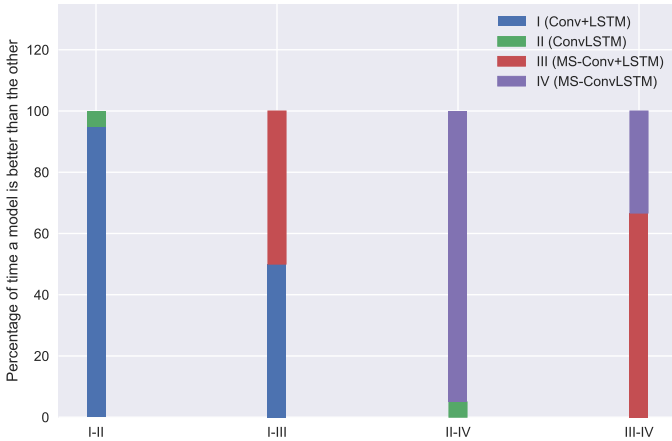


**Figure 4:** Pairwise comparison between the proposed four models to determine the most suitable input representation as well as the best recurrent convolutional configuration. Here, for the sake of simplicity, each model is referred by its corresponding roman letter.

The training time of the four proposed models are displayed in Fig. 5. The training time of the second and fourth models is largely affected by the ConvLSTM layers. More specifically, the significant training time of the MS-ConvLSTM model is affected by the ConvLSTM units in each stream. Moreover, using a multi-stream approach for the stacked recurrent convolutional architecture increases the training time by approximately 44%. Performing the same process on the ConvLSTM architecture raises the training time by 59%.

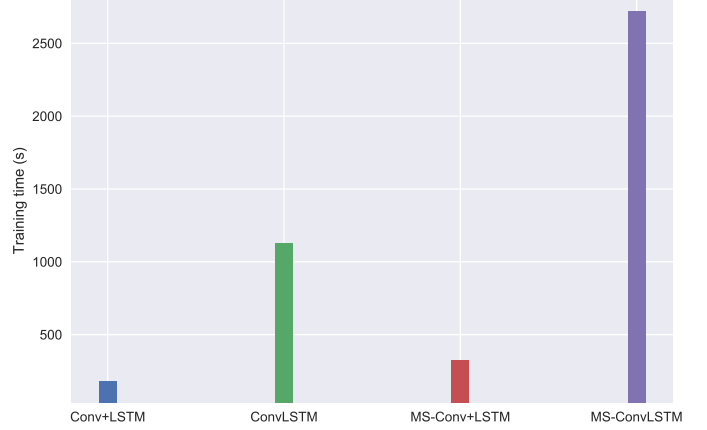


**Figure 5:** Comparison of training time of the proposed approaches.

## 7. Discussion

### 7.1. Network visualization

An effective way to understand which input features and cities affect the outputs is using the techniques explained in sections 3.2 and 3.3. In this section, we present the results of spatial and temporal occlusion analysis and score maximization techniques for the Conv+LSTM and MS-Conv+LSTM models, since these models use different input representations. In addition, for this analysis the models have been trained to predict six days ahead.

#### 7.1.1. Occlusion analysis

In order to determine which features contribute the most to a minimal error between the actual data and the prediction for a particular city, we first determine the MSE between the prediction of a sample and the actual data, which is used as a reference MSE. We then use a mask vector  $m_f \in \mathbb{R}^{1 \times F}$  which is used in a sliding fashion across all the feature rows of the input data. We make an inference everytime  $m_f$  masks a row, compute the corresponding MSE and finally obtain the percentage change between this MSE and the reference MSE. We repeat the same process along all row features to obtain all the percentage change for that particular data sample. The masked row feature that leads to the biggest MSE increase corresponds to the most important feature. Moreover, we repeat the same computations using multiple data samples and we average the percentage changes for each feature row. The same process applies to the rest of the other cities in order to obtain their corresponding important features. On the other hand, to determine the most important cities, we use the same algorithm, but with a mask vector  $m_c \in \mathbb{R}^{C \times 1}$  that is slid across all the column cities of the input data.

Fig. 6 shows the most important features and cities of the Conv+LSTM model after performing the occlusion analysis. This model was trained on the 6 target cities described above with the wind speed as target feature. Fig. 6 (a) shows the most important features for each target city while Fig. 6 (b) presents the most relevant cities for each target city. The wind speed



of London is affected by multiple weather features mostly related to the dew and the temperature. Moreover, there seems to be an agreement about the wind gust as an important weather feature for the prediction of wind speed. Concerning the most critical cities for the wind speed of the target cities, most cities are influenced by nearby cities, and Amsterdam seems to play a critical role, as it is near the sea and close to multiple target cities.

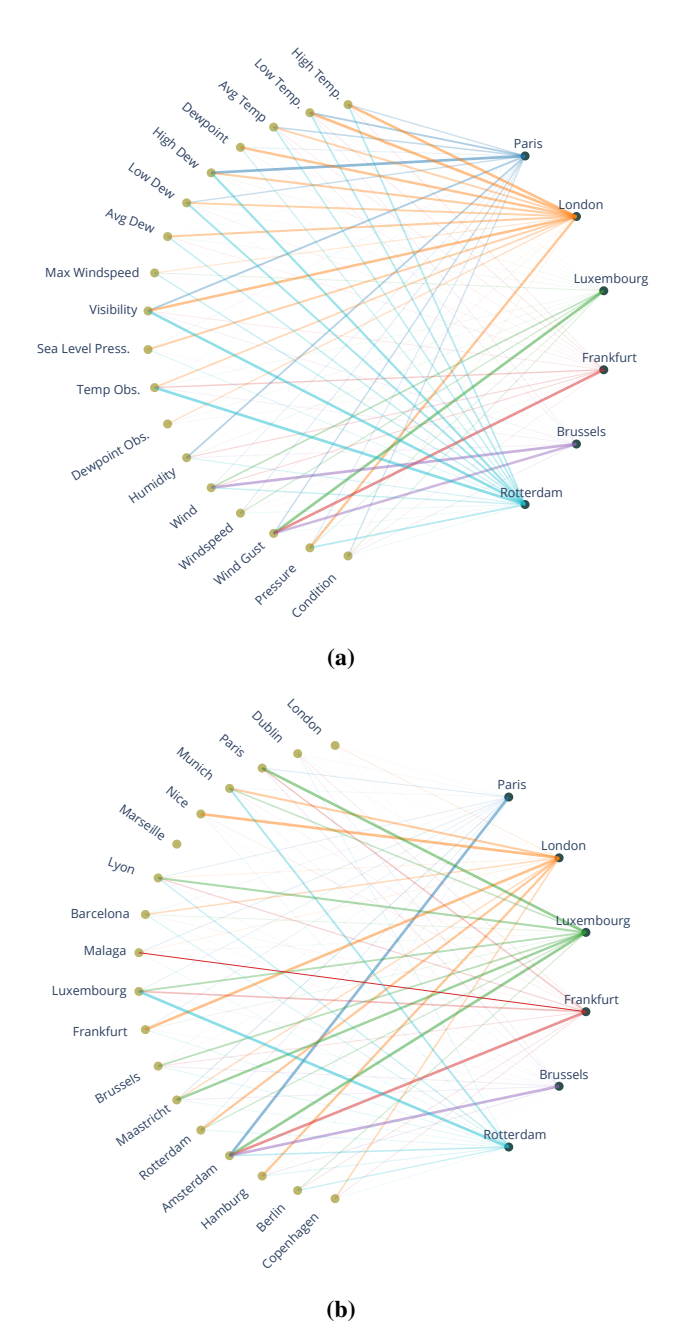


**Figure 6:** Occlusion analysis visualization of the Conv+LSTM model showing the most relevant weather features (a) and cities (b) for each target city. The model was trained to predict the wind speed.

Fig. 7 presents the same information as in Fig. 6, but for the MS-Conv+LSTM model, with the average temperature as target feature. Interestingly enough, the maximum wind speed

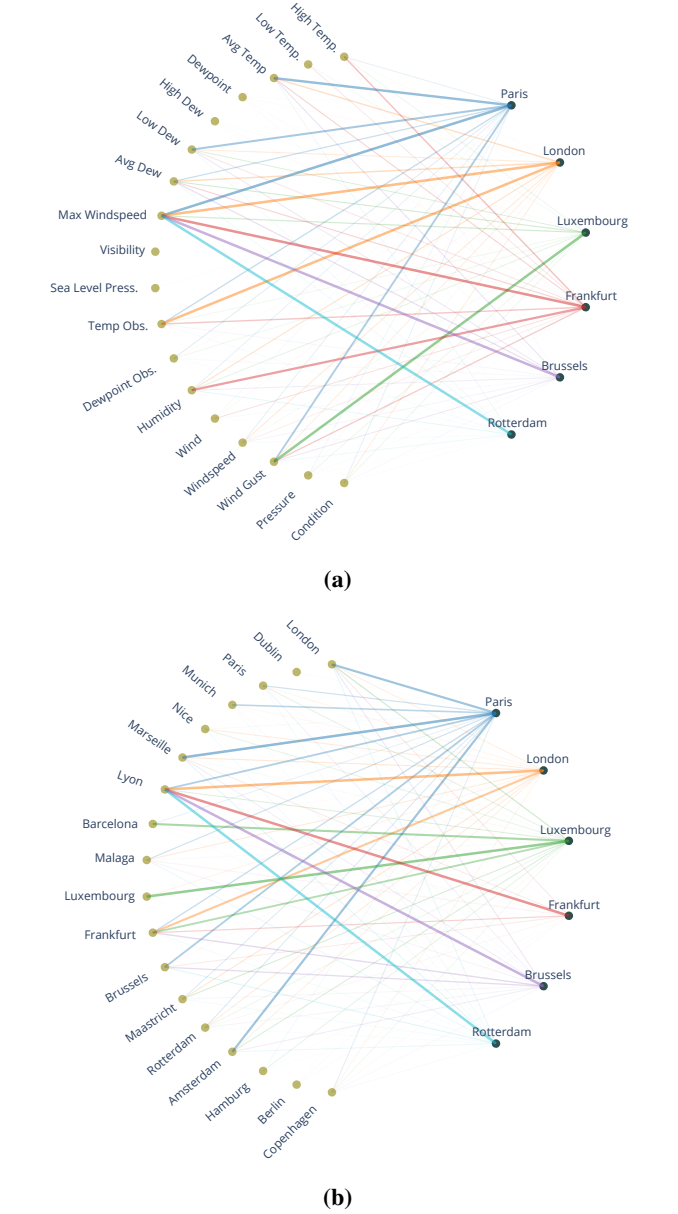


**Figure 7:** Occlusion analysis visualization of the MS-Conv+LSTM model showing the most relevant weather features (a) and cities (b) for each target city. The model was trained to predict the average temperature.

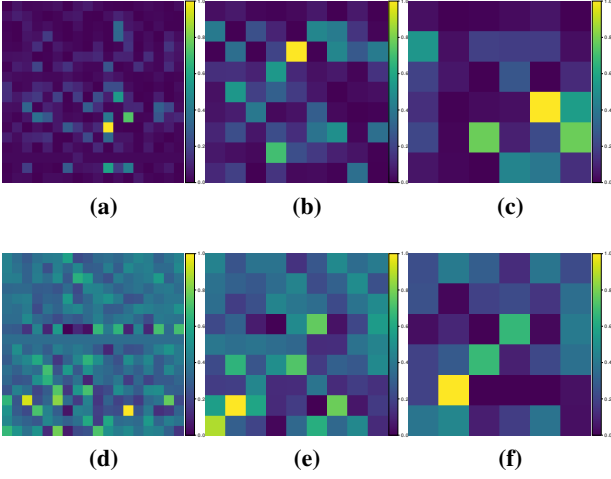


**Figure 8:** Results of the spatial occlusion analysis using different mask sizes. (a,d): mask size  $1 \times 1$ . (b,e): mask size  $2 \times 2$ . (c,f): mask size of  $3 \times 3$ . For both Conv+LSTM and MS-Conv+LSTM models, the target cities are (a,b,c) Rotterdam and (d,e,f) Paris. The Conv+LSTM and MS-Conv+LSTM models were trained to predict the wind speed and temperature, respectively.

plays a major role in these predictions. The temperature observed and the wind gust also seem important, but to a lesser extent. Moreover, the city of Lyon is also critical to the average temperature prediction of the target cities.

Apart from determining the important features or cities only, occlusion analysis can also be useful to determine whether a group of cities or features is important as well. We applied the same process described above, however instead of using vector masks, we used square patch matrices that are slid along both the rows and columns directions, without overlapping. Fig. 8 shows the visualization of this occlusion analysis, where the reference MSE corresponds to the error between the prediction and the actual data of the cities of Rotterdam (a,b,c) and Paris (d,e,f). The top and bottom rows show the visualization of this analysis for the Conv+LSTM and MS-Conv+LSTM models, respectively. The first, second and third columns use patch sizes of  $1 \times 1$ ,  $2 \times 2$ , and  $3 \times 3$ , respectively. Brighter colors correspond to features and cities that are more important. While occlusions shown in subfigures (a), (b), (c), and (f) seem more decisive about the important features and cities, it is less the case for the rest of the subfigures since these maps are generally brighter. For the Conv+LSTM, it is the occlusion done with a patch size of  $3 \times 3$  that provides additional information from the previous analysis, since the most relevant weather features include the temperature observed and the meaningful cities are the adjacent ones (i.e. Maastricht, Rotterdam, Amsterdam). An additional remark about the MS-Conv+LSTM is that the patch size of  $2 \times 2$  is the one that confirms the previous analysis about the important features and cities of this model. Indeed, according to subfigure (e), the most important cities and features to predict the average temperature of Paris are the features wind gust and wind speed, and the cities of Paris and Munich.

Fig. 9 displays the visualization of the temporal occlusion analysis where brighter values mean more relevant lags. As

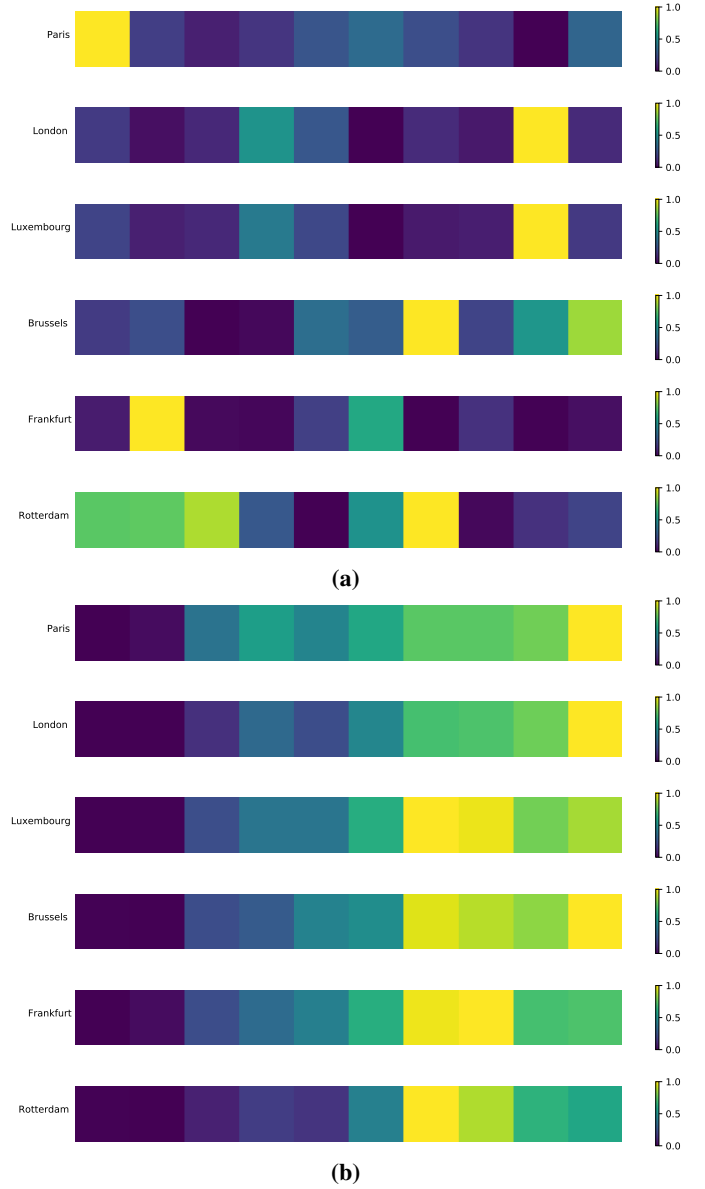


**Figure 9:** Temporal occlusion analysis visualization of the Conv+LSTM (a) and MS-Conv+LSTM (b) models. The Conv+LSTM and MS-Conv+LSTM models were trained to predict the wind speed and temperature, respectively.

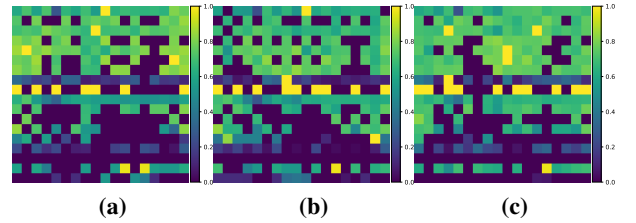


**Figure 10:** Score maximization maps of the Conv+LSTM for the 1<sup>st</sup> (a), 5<sup>th</sup> (b), and 10<sup>th</sup> (c) lags. This model was trained to predict the wind speed.



previously mentioned, this approach aims at finding which lag contributes the most to a minimal error between the actual and prediction data. The leftmost region corresponds to the oldest lags while the rightmost one are the most recent lags. For the model that uses a tensorial representation, Fig. 9 (a), there is no clear pattern since some lags might be important for some specific cities only. However, for the MS-Conv+LSTM model in Fig. 9 (b), the more recent lags yield consistently highest importance. For the cities of Paris, London, and Brussels, the most recent lag is the most critical, while for the rest of the cities, it fluctuates between the 4th most recent or the 3rd most recent lag.

### 7.1.2. Score maximization

Here we show the visualization of the score maximization introduced in section 3.2. Fig. 11 illustrates the score maximization of the Conv+LSTM trained to predict the wind speed for six days ahead. Fig. 11 (a), (b), and (c) refer to the visualization of the score maximization corresponding to model trained with lag = 1, 5, and 10 respectively. One should also note that the first and last lags in the input representation concern the oldest and most recent lags in time, respectively. From a general perspective, these visualizations are harder to interpret than the ones of the occlusion analysis since only subfigure (c) that corresponds to lag 10 depicts a discernable pattern, where the pressure seems like the most crucial weather feature.

Fig. 10 are the score maximization maps that show the relevant weather features for all the cities of the Conv+LSTM model, trained to predict six days ahead daily wind speed. Higher pixel values in the score maps refer to a more important city-feature pair. There is no discernible pattern except the consistent feature across the three lags. This weather feature is the visibility.

## 8. Conclusion

In this paper, four deep neural networks architectures have been proposed and investigated to perform weather elements forecasting. From the analysis of the experimental results, it has been shown that a multi-stream input representation is more suitable for this task. Concerning the recurrent convolutional configuration, the cascaded configuration yielded superior results compared to the one using ConvLSTM layers. In addition, interpretability techniques such as occlusion analysis and score maximization have been used to extract the most relevant input features (i.e. weather features and cities). These methods revealed that in general, neighbouring cities of the target ones can have an impact on the weather target prediction. It has also been shown that wind gust, dew and temperature are important features for the prediction of the wind speed while the maximum wind speed, the wind gust, and the temperature observed heavily influences the daily average temperature. From a temporal perspective, the analyzed models exhibit a clear pattern when it comes to the most important lags. While the tensorial representation do not favor a specific lag, the multi-stream approach uses the

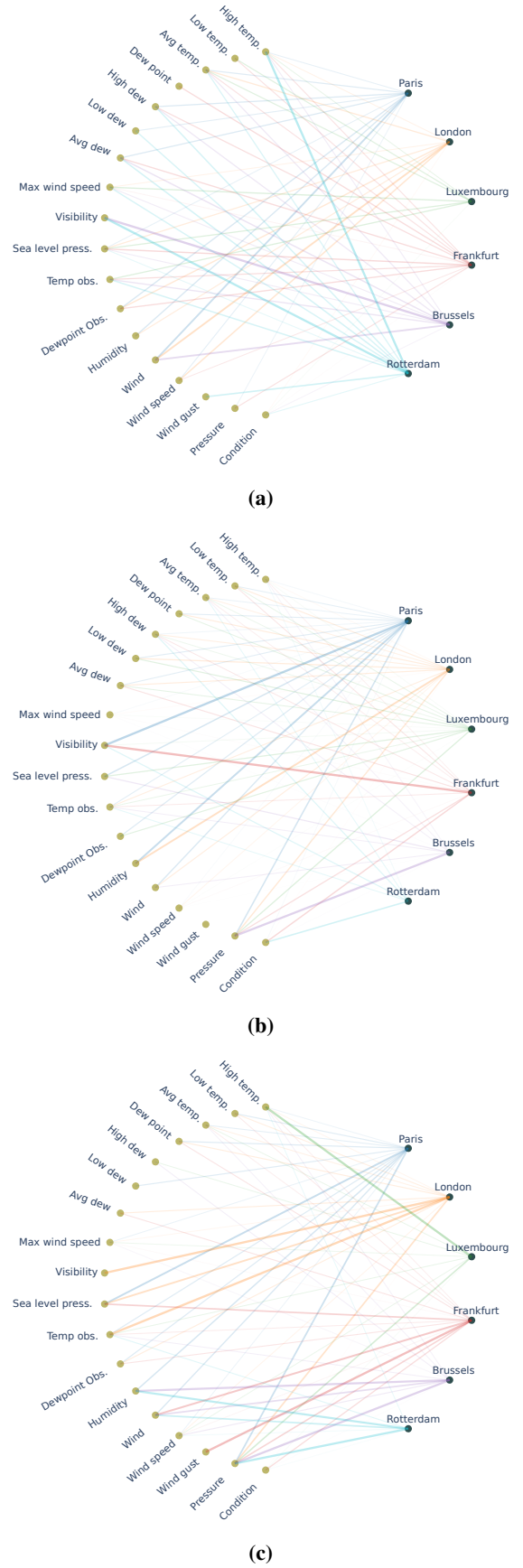


**Figure 11:** Score maximization visualization of the MS-Conv+LSTM for the 1<sup>st</sup> (a), 5<sup>th</sup> (b), and 10<sup>th</sup> (c) lags. This model was trained to predict the average temperature.

most recent lags for its prediction. The data and code used can be found at [github.com/IsmailAlaouiAbdellaoui/weather-forecasting-explained-recurrent-convolutional-nn](https://github.com/IsmailAlaouiAbdellaoui/weather-forecasting-explained-recurrent-convolutional-nn).

## Acknowledgment

Simulations were performed with computing resources granted by RWTH Aachen University and Cloud TPUs from Google's TensorFlow Research Cloud (TFRC).

## References

- [1] Alaoui Abdellaoui, I., García Fernández, J., Şahinli, C., Mehrkanon, S., 2020. Deep brain state classification of meg data. *arXiv preprint arXiv:2007.00897*.
- [2] Bauer, P., Thorpe, A., Brunet, G., 2015. The quiet revolution of numerical weather prediction. *Nature* 525, 47–55.
- [3] Booz, J., Yu, W., Xu, G., Griffith, D., Golmie, N., 2019. A deep learning-based weather forecast system for data volume and recency analysis, in: 2019 International Conference on Computing, Networking and Communications (ICNC), IEEE. pp. 697–701.
- [4] Breiman, L., 2001. Random forests. *Machine learning* 45, 5–32.
- [5] Campbell, S.D., Diebold, F.X., 2005. Weather forecasting for weather derivatives. *Journal of the American Statistical Association* 100, 6–16.
- [6] Chen, R., Wang, X., Zhang, W., Zhu, X., Li, A., Yang, C., 2019. A hybrid cnn-lstm model for typhoon formation forecasting. *Geoinformatica* 23, 375–396.
- [7] Dueben, P.D., Bauer, P., 2018. Challenges and design choices for global weather and climate models based on machine learning. *Geoscientific Model Development* 11, 3999–4009.
- [8] Fu, Q., Niu, D., Zang, Z., Huang, J., Diao, L., 2019. Multi-stations' weather prediction based on hybrid model using 1d cnn and bi-lstm, in: 2019 Chinese Control Conference (CCC), IEEE. pp. 3771–3775.
- [9] Glahn, H.R., 1985. Statistical weather forecasting.
- [10] Gneiting, T., Raftery, A.E., 2005. Weather forecasting with ensemble methods. *Science* 310, 248–249.
- [11] Ho, J., Kalchbrenner, N., Weissenborn, D., Salimans, T., 2019. Axial attention in multidimensional transformers. *arXiv preprint arXiv:1912.12180*.
- [12] Holtzlag, A., De Bruijn, E., Pan, H., 1990. A high resolution air mass transformation model for short-range weather forecasting. *Monthly Weather Review* 118, 1561–1575.
- [13] Kim, S., Hong, S., Joh, M., Song, S.k., 2017. Deepbrain: ConvLstm network for precipitation prediction using multichannel radar data. *arXiv preprint arXiv:1711.02316*.
- [14] Kingma, D.P., Ba, J., 2014. Adam: A method for stochastic optimization. *arXiv preprint arXiv:1412.6980*.
- [15] Lorenc, A.C., 1986. Analysis methods for numerical weather prediction. *Quarterly Journal of the Royal Meteorological Society* 112, 1177–1194.
- [16] Mahendran, A., Vedaldi, A., 2016. Visualizing deep convolutional neural networks using natural pre-images. *International Journal of Computer Vision* 120, 233–255.
- [17] Mehrkanon, S., 2019a. Cross-domain neural-kernel networks. *Pattern Recognition Letters* 125, 474–480.
- [18] Mehrkanon, S., 2019b. Deep neural-kernel blocks. *Neural Networks* 116, 46–55.
- [19] Mehrkanon, S., 2019c. Deep shared representation learning for weather elements forecasting. *Knowledge-Based Systems* 179, 120–128.
- [20] Mehrkanon, S., Falck, T., Suykens, J.A., 2012. Approximate solutions to ordinary differential equations using least squares support vector machines. *IEEE transactions on neural networks and learning systems* 23, 1356–1367.
- [21] Mehrkanon, S., Mehrkanon, S., Suykens, J.A., 2014. Parameter estimation of delay differential equations: an integration-free ls-svm approach. *Communications in Nonlinear Science and Numerical Simulation* 19, 830–841.
- [22] Mehrkanon, S., Suykens, J.A., 2015. Learning solutions to partial differential equations using ls-svm. *Neurocomputing* 159, 105–116.
- [23] Mehrkanon, S., Suykens, J.A., 2018. Deep hybrid neural-kernel networks using random fourier features. *Neurocomputing* 298, 46–54.
- [24] Molnar, C., 2020. *Interpretable Machine Learning*. Lulu. com.
- [25] Niziol, T.A., Snyder, W.R., Waldstreicher, J.S., 1995. Winter weather forecasting throughout the eastern united states. part iv: Lake effect snow. *Weather and Forecasting* 10, 61–77.
- [26] O'Neill, B.C., Oppenheimer, M., Warren, R., Hallegatte, S., Kopp, R.E., Pörtner, H.O., Scholes, R., Birkmann, J., Foden, W., Licker, R., et al., 2017. Ipcc reasons for concern regarding climate change risks. *Nature Climate Change* 7, 28–37.
- [27] Scher, S., 2018. Toward data-driven weather and climate forecasting: Approximating a simple general circulation model with deep learning. *Geophysical Research Letters* 45, 12–616.
- [28] Sønderby, C.K., Espeholt, L., Heek, J., Dehghani, M., Oliver, A., Salimans, T., Agrawal, S., Hickey, J., Kalchbrenner, N., 2020. Metnet: A neural weather model for precipitation forecasting. *arXiv preprint arXiv:2003.12140*.
- [29] Tolstykh, M., Frolov, A., 2005. Some current problems in numerical weather prediction. *Izvestiya Atmospheric and Oceanic Physics* 41, 285–295.
- [30] Trebing, K., Mehrkanon, S., 2020a. Smaat-unet: Precipitation nowcasting using a small attention-unet architecture. *arXiv preprint arXiv:2007.04417*.
- [31] Trebing, K., Mehrkanon, S., 2020b. Wind speed prediction using multidimensional convolutional neural networks. *arXiv preprint arXiv:2007.12567*.
- [32] Webb, S., 2018. Deep learning for biology. *Nature* 554.
- [33] Xingjian, S., Chen, Z., Wang, H., Yeung, D.Y., Wong, W.K., Woo, W.c., 2015. Convolutional lstm network: A machine learning approach for precipitation nowcasting, in: *Advances in neural information processing systems*, pp. 802–810.
- [34] Zhou, K., Zheng, Y., Li, B., Dong, W., Zhang, X., 2019. Forecasting different types of convective weather: A deep learning approach. *Journal of Meteorological Research* 33, 797–809.